



HAL
open science

Fibular registration using surface matching in navigation-guided osteotomies: a proof of concept study on 3D-printed models

Marie de Boutray, João Cavalcanti Santos, Adrien Bourgeade, Michael Ohayon, Pierre-Emmanuel Chammas, Renaud Garrel, Philippe Poignet, Nabil Zemiti

► To cite this version:

Marie de Boutray, João Cavalcanti Santos, Adrien Bourgeade, Michael Ohayon, Pierre-Emmanuel Chammas, et al.. Fibular registration using surface matching in navigation-guided osteotomies: a proof of concept study on 3D-printed models. *International Journal of Computer Assisted Radiology and Surgery*, 2022, 17, pp.1321-1331. 10.1007/s11548-022-02608-0. lirmm-03639410

HAL Id: lirmm-03639410

<https://hal-lirmm.ccsd.cnrs.fr/lirmm-03639410>

Submitted on 12 May 2023

HAL is a multi-disciplinary open access archive for the deposit and dissemination of scientific research documents, whether they are published or not. The documents may come from teaching and research institutions in France or abroad, or from public or private research centers.

L'archive ouverte pluridisciplinaire **HAL**, est destinée au dépôt et à la diffusion de documents scientifiques de niveau recherche, publiés ou non, émanant des établissements d'enseignement et de recherche français ou étrangers, des laboratoires publics ou privés.

Fibular registration using surface matching in navigation-guided osteotomies: a proof of concept study on 3D-printed models

Marie de Boutray^{1,2} . Joao Cavalcanti Santos² . Adrien Bourgeade² . Michael Ohayon² .
Pierre-Emmanuel Chammas^{2,3} . Renaud Garrel¹ . Philippe Poignet² . Nabil Zemiti²

Affiliations:

1. Department of ENT, Neck Surgery and Maxillofacial Surgery, Gui de Chauliac University Hospital, Montpellier, France.
2. LIRMM, University of Montpellier, CNRS, Montpellier, France.
3. Department of Orthopedic Surgery, Lapeyronie University Hospital, Montpellier, France.

Corresponding author:

Marie de Boutray
m-deboutray@chu-montpellier.fr
orcid.org/0000-0003-4571-5774

Abstract (278 words)

Purpose Fibula free flap is currently used in mandibular reconstruction. The main difficulties involved in this surgery concern mandible shaping, and therefore osteotomy positioning on the fibula. The use of navigation could help in osteotomy positioning, but accurate registration is required. We assess a surface-matching method for fibula registration that relies on an iterative closest point (ICP) algorithm. Since the fibula shape is landmark free, a robust registration initialization approach is used to avoid non-optimal local minimums in the ICP.

Methods Bone surface-matching registration was evaluated on a 3D printed fibula and compared to its virtual reference model. The registration initialization relied on 3 initialization points placed on the surgically exposed area, geometrically remote from the fibular distal extremity. The bone surface was digitized and the obtained point clouds were registered to the virtual reference model. The position of 3 assessment points engraved on the 3D printed fibula was then compared to that of the equivalent points on the virtual model.

Results The registration procedure was performed 24 times by an expert surgeon. Seventy two TRE (Target Registration Errors) were computed, corresponding to the distance between the paired assessment points. Most TRE (86.1%) were less than 1 mm, with a maximum of 1.552 mm. The overall mean value was 0.759 ± 0.302 mm.

Conclusion This study illustrates a surface-matching approach for fibula registration, with an initialization method based on points remote from the fibula distal extremity. This registration technique gave promising results and should be considered as a valid registration method for straight bones like the fibula. These findings indicate that navigation can be used for fibula flap shaping for mandibular reconstruction, with a noninvasive and accurate registration method.

Keywords fibula registration . bone surface matching . fibula flap . navigation . mandibular reconstruction . computer-assisted surgery.

Words count: 4741 words

Acknowledgements:

This work was supported in part by the French National Agency for Research (Agence Nationale pour la Recherche, ANR) within the 'Investissements d'Avenir' program (Labex CAMI, ANR-11-LABX0004; Labex NUMEV, ANR-10-LABX-20, and the ROBOTEX Equipex, ANR-10-EQPX-44-01). The authors would like to thank Thibault de Boutray, Noura Faraj and David Berry who kindly helped us with the writing of this paper.

Introduction

Mandibular reconstruction with free fibula flap (FFF) has—since first being reported by Hidalgo in 1988—become a gold standard in reconstructive surgery [1]. The main difficulty of this surgery is in designing and fixing the fibula in the appropriate position to restore mandibular functions and facial aesthetics. Indeed, the fibula must be modelled, and therefore cut into several fragments, in order to restore the curvilinear shape of the mandible. The precision of the position and orientation of the fibular planes of cuts (called osteotomies) directly impacts the mandibular reconstruction and reossification results [2,3]. The surgical learning curve to restore the 3D mandibular shape with this FFF is substantial as experience on 60-100 flaps is necessary to achieve a 95% success rate [4]. This 95% rate means that it could take from 1 to more than 5 years, depending on the number of flaps conducted per year.

Several solutions using computer-aided design (CAD) and computer-aided manufacturing (CAM) techniques have been proposed to guide osteotomy positioning on the fibula [5,6,7]. But these CAD and CAM techniques have the disadvantage of being expensive and time-consuming. The position and orientation of osteotomies on the fibula could thus be guided by surgical navigation. Navigation is routinely applied in many medical fields, especially in surgery. It helps guide the surgical procedure after preoperative virtual planning based on the patient's medical imaging findings. The accuracy of the procedure largely depends on the accuracy with which the patient can be registered to this virtual planning [8,9]. In the specific field of mandibular reconstruction, navigation has been applied for mandibular shape reconstruction guidance [10-12], but seldom to guide fibular osteotomies [8,13]. Surgical navigation would be easily applicable in this indication, but it requires a reliable registration method to guarantee its accuracy.

Overall, there are two types of registration methods: (i) landmark- and (ii) surface-based methods [9,14]. Regarding the former method (i), landmarks can be either anatomical or artificial. In the FFF context, the fibular bone surface is homogeneous and quite featureless, thereby hampering the definition of anatomical landmarks. Artificial landmarks can be set by anchoring a transcutaneous fiducial marker on the fibula and imaging it with a preoperative computed tomography (CT). However, this method remains invasive, painful and uncomfortable for the patient if the fiducials are placed before the surgery. Fiducial marker anchoring and imaging may also be performed intraoperatively, but would thus require an intraoperative CT, which is only available in a few medical centers [15].

We hence opted for the surface-based registration method (ii), which is less invasive than the artificial landmark-based method. This method relies on registration between the digitized surface of the patient and the corresponding one on the preoperative reference CT. The registration is performed using an iterative closest point (ICP) surface matching procedure.

Due to the fibula shape and its homogeneous surface, it does not present any anatomical landmark on its surgically exposed area (SEA) that could be used as keypoints for the registration initialization (Fig. 1). A conventional ICP-based registration procedure could therefore fail by converging to local minima that are not globally optimal solutions. We attempted to solve this registration initialization issue by defining initialization keypoints located on the SEA region and geometrically remote from a palpable anatomical landmark. We therefore used its distal extremity, which is the only palpable anatomical landmark on the fibula. We have named these initialization keypoints: 'remote initialization points' (RIPs).

The main contribution of this study is the design and introduction of the RIP approach and its experimental validation using a 3D printed fibular model. This RIP approach is a key step in the bone surface-matching registration method assessed here.

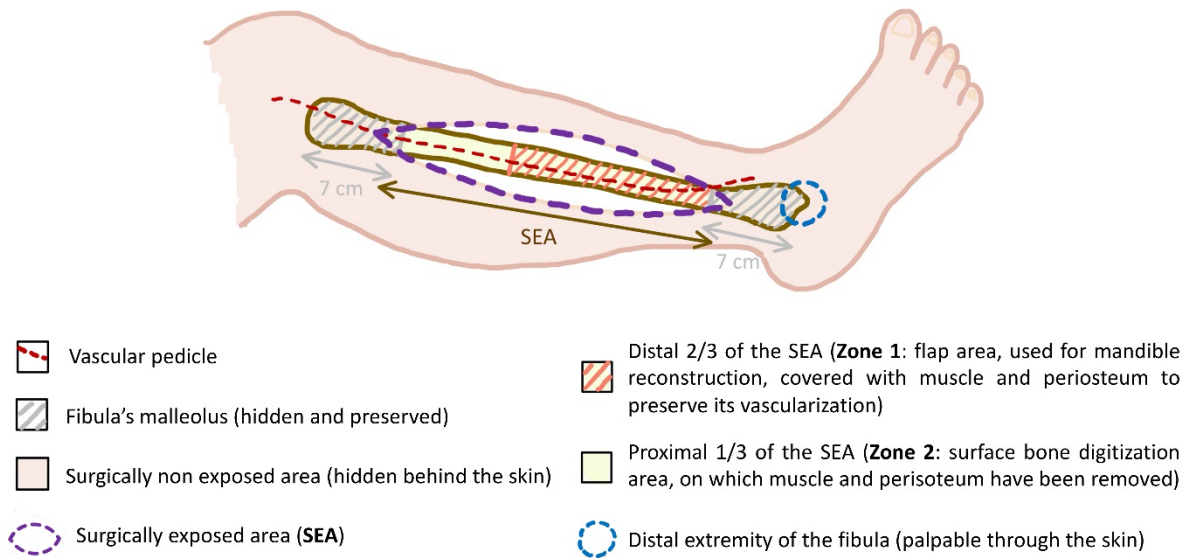


Fig. 1 Exposure of the fibula in clinical practice: the purple dotted area is the surgically exposed area (SEA), which is the part of the fibula not hidden under the skin. The rest of the fibula (the malleolus) is hidden. The SEA is straight and homogeneous and corresponds to the diaphysis of the fibula

Material and methods

We assessed the accuracy of the proposed bone surface-matching registration method using a 3D-printed fibular model created from a preoperative CT (resolution $710 \times 710 \times 625 \mu\text{m}^3$) of a human leg. The DICOM images were segmented manually to generate a 3D mesh fibular model (named 'virtual model' and composed of 5756 vertices and 11508 faces). The segmentation was achieved using the 3D Slicer software [16] with threshold set between 560 HU and 1943 HU (Hounsfield Unit), and no smoothing.

We added a tracked marker to this fibular virtual model (Fig. 2) so as to be able to spatially track the fibula position and freely manipulate it during and after registration.

This marker was fixed on the fibula distal malleolus and did not interfere with the SEA.

Finally, 3 assessment points were defined and engraved in the mesh model, on the fibula body to allow evaluation of the registration procedure.

This 3D fibular model was 3D printed in polylactic acid (PLA) using a 3D desktop printer (Raise3D® N2 plus). We used the following printing parameters: 0.10 mm layer thickness, 0.0125 mm positioning resolution on the X/Y axis and a 100% infill. We named this 3D printed fibular model: 'physical model'.

In a clinical setting, the physical model would correspond to the patient's fibula, and the virtual model would correspond to the patient's CT scan.

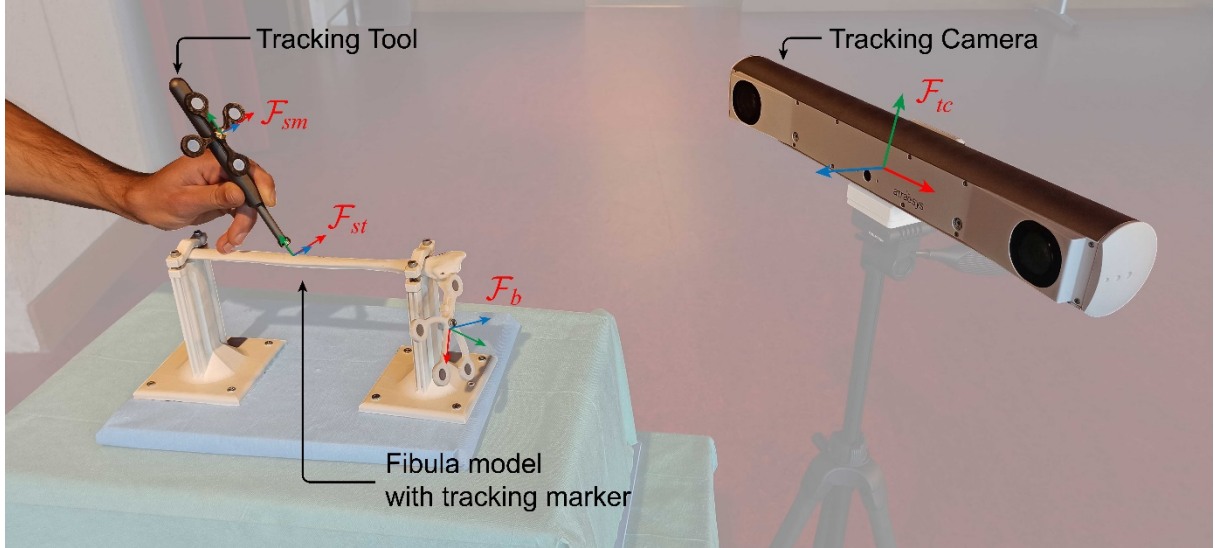


Fig. 2 Fibular navigation experimental setup with the defined coordinate frames: the fibula physical model with its tracked marker (\mathcal{F}_b), the stylus tool with its tracked marker (\mathcal{F}_{sm}) and tip (\mathcal{F}_{st}) and the tracking camera (\mathcal{F}_{tc})

Navigation system and tracked tool calibration

The navigation system used was the optical FusionTrack 500 tracking camera and system (Atracsys®, Switzerland, accuracy 0.09 mm RMS up to 2m away). Point acquisition was performed on the 3D printed fibula (physical model) using a tracked tool (a stylus with a marker) with a 1.27 mm sphere at the tip. The remote center of motion (sphere center at the tracked stylus tip) was calibrated before each trial using the ATS method [17]. As the calibration was achieved at the center of the tip sphere, the acquired points were offset from the fibula surface, by the radius of the sphere (0.635 mm). In order to compensate for this offset, we added 0.635 mm along the normals of the digitized point cloud (corresponding to the radius of the sphere at the tip) [9].

\mathcal{F}_{st} was the frame attached to the tracked stylus tip and \mathcal{F}_{sm} , the frame attached to the stylus marker. The position ${}^b\mathbf{P}_i$ of each i^{th} point acquired on the ‘bone’ (fibula physical model) was expressed in the frame \mathcal{F}_b attached to the bone marker (Fig. 2). This ${}^b\mathbf{P}_i$ position was then obtained via the following transformation:

$${}^bT_{st,i} = ({}^{tc}T_b)^{-1} \times {}^{tc}T_{sm} \quad {}^{sm}T_{st}$$

defined by:

$${}^bT_{st,i} = \begin{bmatrix} {}^bR_{st,i} & {}^b\mathbf{P}_i \\ 0 & 1 \end{bmatrix}$$

where:

${}^{sm}T_{st}$ denotes the transformation from \mathcal{F}_{st} to \mathcal{F}_{sm} obtained using the stylus ATS calibration method

${}^{tc}T_{sm}$ is the measured transformation from \mathcal{F}_{sm} to the optical tracker reference frame \mathcal{F}_{tc}

${}^{tc}T_b$ is the measured transformation from \mathcal{F}_b to \mathcal{F}_{tc}

${}^bT_{st}$ is the transformation from \mathcal{F}_{st} to \mathcal{F}_b and ${}^bR_{st}$ is the corresponding rotation matrix.

Registration initialization

A fibula is a long bone without any specific anatomical landmarks or topography other than its malleolus (Fig. 1), which could be accurately identified and used as a navigation reference. But, in order to preserve the stability of the ankle joint, the fibula malleolus is not exposed during the surgery and fibula flap is then detached from it. Once detached, the flap can be cut and designed in the appropriate position to restore the mandibular shape. The resulting SEA is thus straight and homogeneous which makes it difficult to find robust initial parameters to execute the standard ICP registration algorithm.

Although the distal fibula malleolus is not exposed during surgery, it can be palpated through the skin. Therefore its distal extremity can be used as a reliable and easily identifiable anatomical landmark before detachment from the fibula SEA. RIPs located on the fibular SEA can thus be defined, geometrically distant from

that distal extremity anatomical landmark.

Here we therefore propose to use those RIPs for the registration initialization step. In clinical practice, the proximal third of the fibular SEA is not included in the flap and can thus be used for bone surfacing. On this specific area, which is usually located around 18-25 cm from the fibular distal extremity, the periosteum and the muscles can be removed from the bone to expose its surface, thereby facilitating bone surfacing. On the 2 remaining thirds of the fibular SEA (Fig. 1), the muscle, periosteum and vessels need to remain attached to the bone to ensure its vascularization. Bone surfacing cannot be achieved in this area.

We thus defined 3 RIPs on the proximal third of the SEA (Fig. 3). The first point (A) was defined on the fibular posterior border, 20 cm away from the distal extremity of the malleolus. The second (B) and third (C) points were defined on the fibular anterior border, respectively 20 cm and 23 cm away from the distal extremity of the malleolus. The positioning of the RIPs on the physical model was determined using a rigid graduated ruler, placed parallel to the length axis of the fibula model. The tracked tool was then placed on either the anterior or posterior border, at 20 or 23 cm, depending on which point was going to be acquired (Fig. 3). On the virtual reference model, three 0.4 mm diameter spheres were drawn by CAD on the virtual fibula mesh, corresponding to the position of each virtual initialization point. The position of those virtual RIPs was determined for each trial by manually clicking the center of each sphere.

The 3 physical RIPs (A, B and C) were digitized for each trial on the 3D printed fibula (physical model) and matched with the corresponding points (A', B' and C') on the virtual model. Each acquired pair of points (A-A', B-B' and C-C') were subsequently used as initialization parameters for each ICP registration procedure. CloudCompare 3D software [18] was used to perform this registration initialization process.

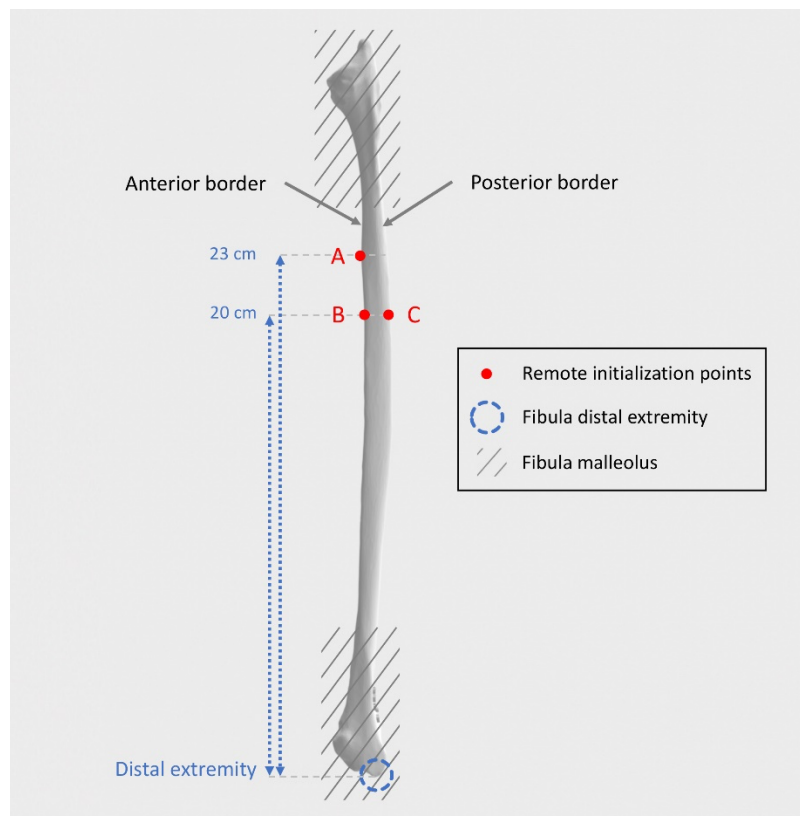


Fig. 3 ICP initialization: 3 RIPs are defined on the fibula: Points A and B located on the anterior border, respectively at 23 and 20 cm from the fibular distal extremity and Point C located on the posterior border 20 cm from the distal extremity

Bone surface reconstruction

After the registration initialization process, bone surface digitization was performed on the proximal third of the fibular SEA, each time following the same technique. The operator was asked to digitize the surface of this area with the tracked tool tip, maintaining the tool marker within the tracking camera field of view. The digitization of the bone surface was achieved on the fibula lateral face with its 2 adjacent borders, over about 15 cm², performing back and forth movements with the tracked tool (Fig. 2 and 4). The tracked tool tip had to be maintained permanently in contact with the fibula. We used this particular technique and performed the digitization on this 15 cm² area, because it is

clinically feasible on a fibula flap. The fibula surface of interest was digitized by homogeneously acquiring around 20,000 points on this zone (Fig. 4). The resulting point cloud was analyzed for registration to the fibula mesh (virtual model) [19]. This bone surface digitization was achieved 24 times (#1 to #24), on the same fibular model by an expert surgeon. The registration procedure was then achieved using the ICP algorithm provided by the CloudCompare 3D software [18] (Fig. 4). This ICP algorithm aimed to find the transformation between the digitized point cloud (digitized physical model) and the reference surface (virtual model mesh), by minimizing the square errors between these two corresponding entities [20] (the digitized point cloud and the mesh). Noting that one of the compared models is a mesh, a point-to-mesh distance computation was then achieved [21-23].

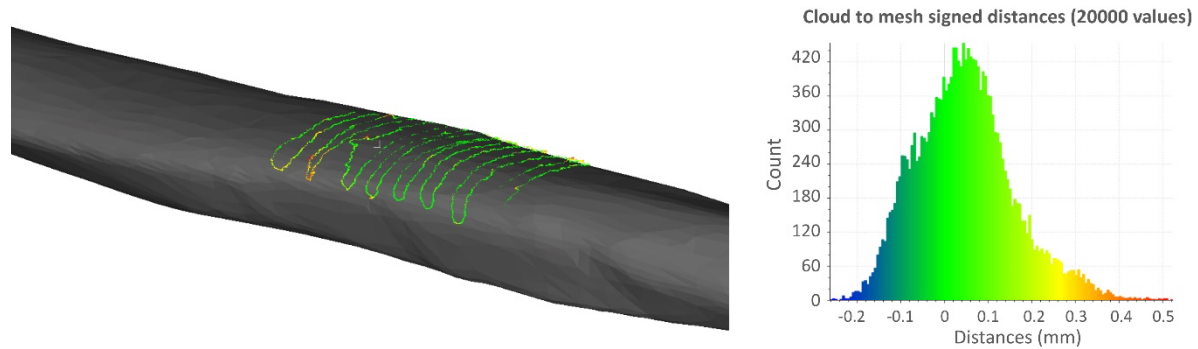


Fig. 4 Registration between the physical fibula's point cloud (in bright colors, obtained by digitization of the fibula surface) and the virtual fibula mesh (in dark grey, obtained after segmentation of the CT scan). The bone surface digitization was achieved on the proximal third of the SEA, performing back and forth movements with the tracked tool tip touching the bone surface. Approximately 20,000 points were acquired on the physical model per procedure. The histogram on the right side, highlights the distribution of the 'cloud to mesh' distances obtained with the ICP algorithm after registration between the digitized point cloud and the virtual model surface

We used the following parameters to set our ICP algorithm: the maximum corresponding distance was 1 mm; the maximum number of iterations that the internal optimization should run for was 100,000; the Transformation Epsilon was 0.1 mm; and we used reciprocal correspondences.

The registration procedure output is the $\mathbb{R}^{4 \times 4}$ transformation matrix ${}^bT_{CT}$ that enables transformation of the fibular virtual model 'CT-scanned frame' F_{CT} to the physical model bone frame F_b . It thus allows computation of the position P_v of any virtual fibula point in the physical bone frame F_b . In clinical practice, this makes it possible to report the virtually planned osteotomies in this physical model frame corresponding to the patient frame.

Performance evaluation

We subsequently assessed the registration accuracy by defining three assessment points on the virtual fibula mesh. Those points were empty half-spheres (0.7 mm radius) designed by CAD on the surface of the virtual fibula (Fig. 5). They were printed as part of the physical model, as defined on the virtual model.

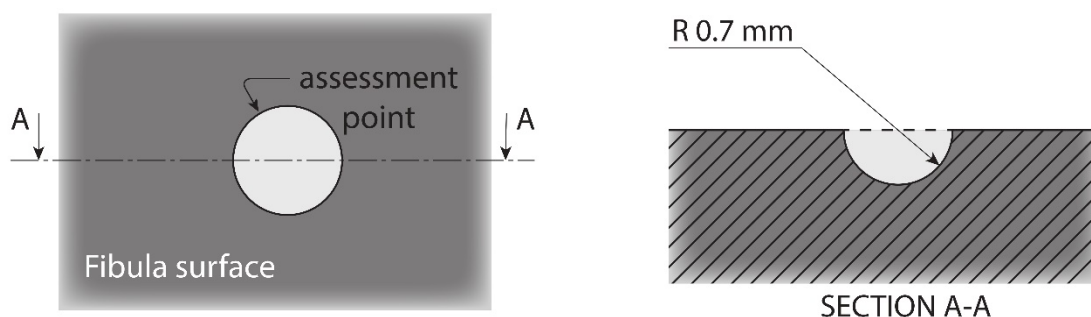


Fig. 5 Design of the assessment points: they were empty half spheres of 0.7 mm radius, designed on the surface of the virtual fibula model and then printed as part of the physical one. On the left: the fibula surface view; On the right: the fibula sectional view through the A-A line

In order to evaluate errors due to deformability (intrinsic elasticity) of the PLA printed fibula, those assessment points were placed in 2 different areas: the distal third (zone 1) and the proximal third (zone 2) of the fibula. Two

physical fibulas have indeed been printed following the same parameters and using the same 3D printer:

- one with its assessment points located in zone 1, in the area where the osteotomies were to be performed (flap area)
- the second with its assessment points located in zone 2, in the area of the bone surface digitization.

The first registration procedures (#1 to #18), were achieved using the fibula with its assessment points in the flap area. The last procedures (#19 to #24), were achieved using the fibula with its assessment points in the area of the bone surface digitization.

Those 3 physical assessment points $\mathbf{P}_{p,i}$ ($i=1,2,3$) were therefore acquired on the fibular physical model after the bone surface reconstruction step using the tracked stylus. The position of the physical assessment points $\mathbf{P}_{p,i}$ was defined by the position of the tracked stylus tip center when positioned in each corresponding half-sphere. The position of the virtual assessment points $\mathbf{P}_{v,i}$ was defined by the position of each half-sphere center. No compensation of the stylus tip radius was then needed for the digitized verification points. To avoid any bias in the results, no feedback was given to the operator at any step of the process.

The registration transformation ${}^bT_{CT}$ was then applied on the position of the virtual assessment points ${}^{CT}\mathbf{P}_{v,i}$ located in the CT-scanned frame, while relocating them on the physical bone frame \mathcal{F}_b . This allowed us to compare their transformed position ${}^b\mathbf{P}_{v,i}$ to the position of the corresponding physical assessment points ${}^b\mathbf{P}_{p,i}$, as follows:

$$\begin{bmatrix} {}^b\mathbf{P}_{v,i} \\ 1 \end{bmatrix} = {}^bT_{CT} \begin{bmatrix} {}^{CT}\mathbf{P}_{v,i} \\ 1 \end{bmatrix}$$

CloudCompare software was then used to compute the distance between the physical digitized assessment points ${}^b\mathbf{P}_{p,i}$ and the corresponding virtual points ${}^b\mathbf{P}_{v,i}$, as represented in the equation below:

$$TRE = \sqrt{({}^b\mathbf{P}_{v,i} - {}^b\mathbf{P}_{p,i})^2}$$

The target registration error (TRE) was defined as the Euclidean distance between the physical and virtual assessment points. Statistical analysis of TRE according to the assessment point positions was performed with a Wilcoxon-Mann-Whitney test. The subgroup analysis comparing the TRE of the 3 assessment points was achieved using an ANOVA test. The threshold of statistical significance for both tests was set at $p < 0.05$.

The procedure is schematized in Figure 6.

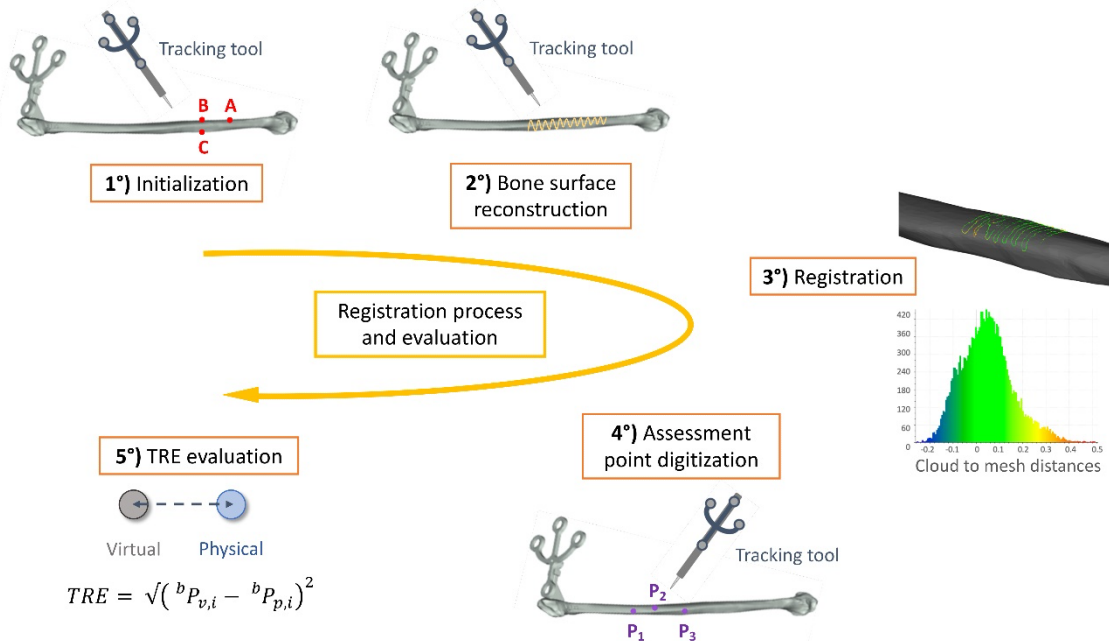


Fig. 6 The 5-step registration process: 1°) Initialization: digitization of RIPs, 2°) Digitization of the bone surface (acquisition of the physical fibula's point cloud), 3°) Pre-registration and registration of the virtual fibula surface (mesh) with the physical fibula's point cloud using the ICP algorithm; 4°) Digitization of the 3 assessment point positions 5°) Evaluation of the method accuracy (Euclidean distance between virtual and physical engraved assessment points)

Results

The registration procedure was performed 24 times on a 3D-printed fibular model.

RIPs, assessment points and the bone surface were collected by an expert surgeon familiar with surgical navigation. Each procedure (from initialization to TRE assessment) lasted 2-6 min. Acquisition of RIPs, the surface point cloud and assessment points could be performed on an immobilized fibula or on a mobile fibula held steady by the physician, via the reference marker fixed on the fibula physical model. Around 20,000 points were digitized during each bone surface reconstruction. The surface matching errors obtained after all 24 ICP registrations with the virtual fibula never exceeded 0.6 mm (Fig. 4).

The results of the 24 registration procedures are shown in Table 1. For the first 18 procedures, the assessment points were located in the flap area (zone 1). For the last 6 procedures, those assessment points were located on the area of the digitized bone surface used for registration (zone 2). 72 TRE were computed (1 TRE per assessment point, which gave 3 TRE per 24 procedures = 72 TRE). Most TRE (86.1% (62/72)) were less than 1 mm (Table 1 and Fig. 7). The remaining 10 ranged from 1.0 to 1.56 mm (TRE with asterisk in Table 1), with a maximum TRE of 1.552 mm for the first point of procedure n°10. The overall mean value for 72 TRE was 0.759 ± 0.302 mm and the median was 0.76 mm. No significant difference was found between TRE of the 3 assessment points (means 0.837 mm, 0.708 mm and 0.731 mm, respectively, $p = 0.2911$).

Table 1 Performance evaluation of the 24 registration procedures (TRE [in mm] defined as the distance between navigated and virtual assessment points)

Procedure	TRE 1rst point	TRE 2nd point	TRE 3rd point	TRE Mean Value	TRE Std Dev
Overall	0.837	0.708	0.731	0.759	0.302
Overall Zone 1	0.895	0.784	0.781	0.820	0.299
1	0.391	0.386	0.423	0.4	0.02
2	0.783	0.499	0.324	0.535	0.232
3	0.914	0.391	0.376	0.56	0.306
4	0.69	0.401	0.838	0.643	0.222
5	0.992	0.561	0.625	0.726	0.233
6	0.884	0.815	0.496	0.732	0.207
7	0.981	0.753	0.956	0.897	0.125
8	0.728	0.706	0.777	0.737	0.036
9	1.538*	1.08*	0.626	1.081	0.456
10	1.552*	1.27*	0.994	1.272	0.279
11	0.869	0.559	0.755	0.728	0.157
12	0.626	0.803	0.94	0.79	0.157
13	0.993	1.41*	0.993	1.132	0.241
14	1.478*	0.97	1.259*	1.236	0.255
15	0.564	0.804	0.773	0.714	0.131
16	0.781	1.178*	0.888	0.949	0.205
17	0.762	0.6	0.938	0.767	0.169
18	0.589	0.923	1.082*	0.865	0.252
Overall Zone 2	0.663	0.482	0.578	0.574	0.230
19	0.524	0.362	0.288	0.392	0.099
20	0.479	0.377	0.586	0.481	0.104
21	0.589	0.399	0.543	0.51	0.099
22	1.087*	0.923	0.86	0.957	0.117
23	0.538	0.306	0.358	0.401	0.122
24	0.758	0.525	0.835	0.706	0.161

Std Dev: standard deviation between the values of the 3 points in a same procedure; Zone 1: procedures for which the assessment points were located on the surgical surface of interest (distal thirds of the fibula); Zone 2: procedures for which the assessment points were located on the area of the bone surface reconstruction (proximal third of the fibula); TRE greater than 1mm are marked with an asterisk

As expected, the subgroup analysis revealed significantly lower TRE for assessment points located in zone 2 (digitized bone surface area, mean 0.574 ± 0.23 mm) compared to those located in the zone 1 (flap area, mean 0.820 ± 0.23 mm; $p < 0.05$). This subgroup analysis confirmed that the error increased with the distance of the

assessment points from the registration area (Fig. 7).

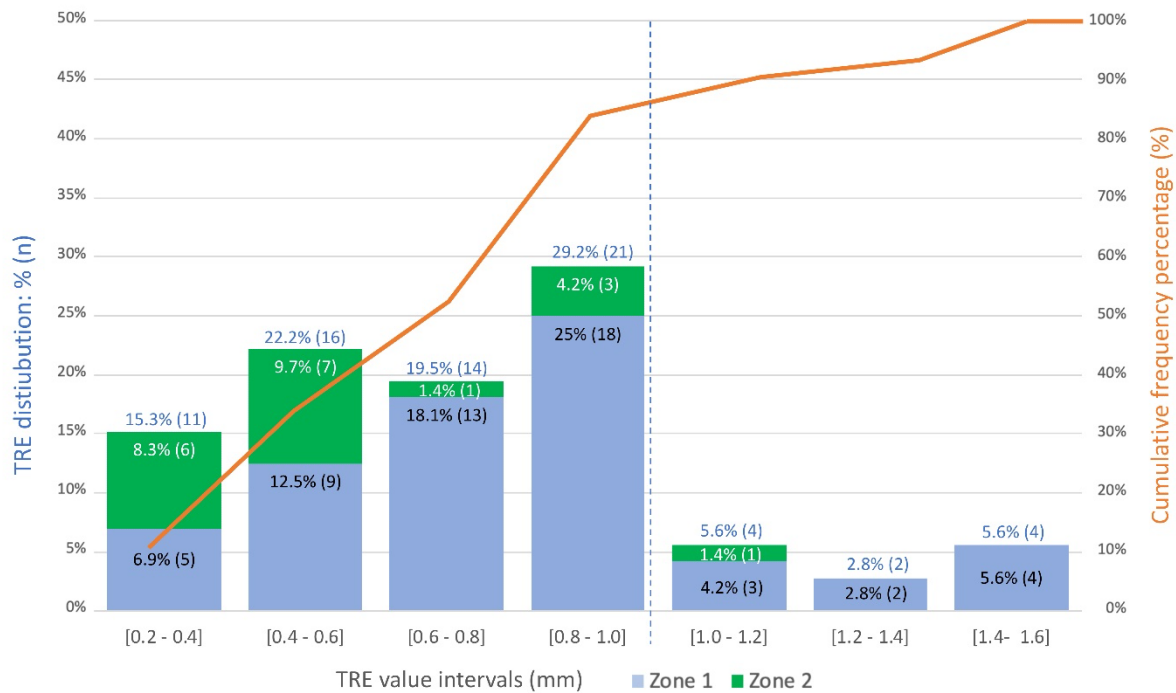


Fig. 7 Distribution of TRE values (n=72). The columns show the TRE distributions according to their value intervals: in light blue the distribution of the TRE related to the assessment points located on the flap area (Zone 1); in green the distribution of that related to the assessment points located on the digitized bone surface area (Zone 2). The orange line represents the cumulative frequency percentage of TRE below each value bracket. 86.1% (62) TRE values were less than 1 mm (dotted blue line)

Discussion

The aim of this study was to demonstrate that bone surface-based registration was possible on the fibular diaphysis despite the absence of anatomical landmarks on it. One of the main difficulties was to find a reliable registration initialization method to avoid the algorithm to fail by converging into local minima. We thus propose a method to define initialization points geometrically remote from the most distal end of the fibular malleolus. This method allowed us to successfully register the 3D printed fibula with its virtual model so as to be able to navigate the fibula osteotomies.

Several techniques are described in the literature to guide osteotomy positioning on the fibula. CAD and CAM techniques can be used to plan patient-specific stereolithographic osteotomy guides and fixation plates from the 3D models of fibular and mandibular anatomy of the patient [5]. This surgical planning can be performed by the medical team using in-house techniques [6,24,25], or by manufacturers according to the surgical team's requirements [7,26]. In-house techniques are time-consuming, the sterilization process is complex, and certification is often not easy to obtain. Guides and plates designed by manufacturers are accurate, specific and easy to use, and their sterilization process is certified. Yet, their cost (estimated at €2,500/patient) and production time (3-6 weeks) limit their usage [27]. Mandibular tumors are the most common causes of mandibular resections. They require quick removal and reconstruction, which are not in line with the several weeks wait to get a manufactured guide.

Beside CAD and CAM techniques, the position and orientation of osteotomies on the fibula could be guided by surgical navigation. However, the accuracy of the navigation is significantly linked to the registration [28]. Our results revealed a mean TRE of 0.759 ± 0.302 mm, which is under the 2 mm surgical accuracy recommended in the literature, thereby meeting clinical requirements [8].

The detailed analysis of the obtained TRE highlighted several points. First, the TRE never exceeded 1.6 mm since its maximum value was 1.55 mm (point located in Zone 1). Higher TRE could derive from the registration process itself but could also be introduced by the operator when pointing and digitizing the assessment points using the tracked pointer. Indeed, a non-rigorous assessment point digitization process could increase the TRE and be responsible for variability between TRE values in the same procedure. For instance, in the 9th procedure, the TRE

of the first assessment point was 1.538 mm whereas that of the second point was 1.08 mm and that of the third point was 0.626 mm. The major gap between those 3 TRE values could not be only explained by the registration method. A reduction of the deviations was obtained for the 6 last acquisitions: the mean standard deviation of the last values was 0.117 [0.099;0.16], whereas the mean standard deviation of the first values was 0.205 [0.02;0.456] ($p = 0.009$). These reduced deviations indicate the existence of a learning curve on the measurement of the assessment points.

We then considered the possibility that the elasticity of the 3D printed models could induce deformation along the fibular diaphysis when touching or surfacing it during the bone surface digitization process. In the first procedures, the assessment points were in the distal part (zone 1) in order to avoid having points printed in the area of the bone surface digitization. But, the sub-group analysis finally highlighted that the TRE of the procedures with zone 2 assessment points, were significantly better than the TRE with assessment points placed in zone 1 (TRE means 0.574 ± 0.23 mm and 0.820 ± 0.23 mm, respectively; $p < 0.05$). The PLA fibula elasticity could lead to its deflection and result in a TRE increase when the assessment points were placed at some distance from the bone surface-marking zone. We therefore quantified the influence of the PLA elasticity on the TRE. More precisely, first, we quantified the average force applied on the fibula during digitization of the points with a force sensor and a stylus, and we obtained a force of approx. 3N. We then used the finite-element analysis procedure in Solidworks® software package (Dassault Systèmes Solidworks, Waltham, USA) to simulate deformation of a 15 cm fibular model in PLA by applying this 3N force at the center of the fibula. The simulation analysis showed an elastic deflection of 0.26 mm, which corresponds to the difference in the order of magnitude between the TRE of zones 1 and 2. In clinical practice, bone is significantly less deformable than PLA, as the elasticity modulus of an adult fibula bone is 8- to 10-fold higher than that of a PLA fibula (26-29 GPa for adult fibula bone [29] versus 3GPa for PLA). The registration accuracy should thus be stable all along the length of the fibula bone, regardless of the distance between the digitized surface and the osteotomy positioning.

A substantial error along the fibula axis could have been expected. Indeed, as the fibula diaphysis is fairly homogeneous and therefore resembles a prismatic surface, a shift in the registration towards either of the fibula extremities would have been probable. However, the TRE analysis did not reveal any particularly significant error on this axis or in any other direction. Our RIP initialization method therefore made it possible to avoid such fibula axis shifts. In ongoing studies, we plan to assess both the impact on the TRE of translating these RIPs along the fibula axis and especially the possible impact of this translation along the fibula axis on the osteotomies.

We highlight that precision during the surface-marking process is a crucial component in the application of the proposed method. The rather irregular surface of the 3D printed fibula used here may therefore have biased the presented results. Clearly, this issue should not arise in the human fibula bone surface-marking process. It could be hoped that the precision would be better when dealing with an actual bone, which presents a smoother surface. The skills necessary to achieve a precise acquisition could be the focus of future research.

We opted to use CAD designed physical assessment points to evaluate the proposed registration method accuracy. We could also have used the tracked marker attached to the fibula to achieve perfect registration. Once obtaining the ground truth using the perfect registration, the accuracy of the registration method could be confirmed by defining virtual points on the SEA as compared with their paired points once the initialization and registration are achieved. Nevertheless, the accuracy of the assessment method would thus be dependent on the accuracy of the fibula tracker, its exact position and its distance from the surface reconstruction area. These data may be inaccurate due to the PLA elasticity (see the aforementioned finite-element method study). We indeed preferred to base the evaluation on the CAD designed assessment points, which are only dependent on the accuracy of the optical tracking device and their digitization process.

The use of navigation in the reconstruction of mandibular defects with fibula flaps have been described [10-12]. Most of them concerned navigation on the mandible rather than on the fibula. No fibular registration was performed in these studies. Navigation was focused on the mandible once the fibula was modelled and transferred to the mandible.

Three studies have been published regarding navigated fibular osteotomies. The first one used the Z-touch Technology (Brainlab, Germany) on the skinned surface of the crus and attached a reference star array on the ankle with a headband [8]. The authors reported an accuracy of < 2 mm with this registration method. In the second study presented in [14], the authors used anchored fiducial markers for intraoperative navigation which were fixed before surgery to the upper part of the fibula. The third study used 3D printed fibular and tibial models with a manufactured lower leg phantom around the bones to mimic skin [13]. The aim of the study was to compare the accuracy of point-pair registration (using skin adhesive markers to serve as registration fiducials) and a hybrid registration (using point-pair and surface matching registration methods). They also assessed the accuracy of navigation guided osteotomies. Although it is difficult to compare these different related studies, these three registration techniques generated errors > 1 mm, which we think is not good enough to achieve satisfactory accuracy in the fibula osteotomy procedure. In the studies of Li et al. [8] and Pietruski et al. [13], the fibula was fixed in relation to the tibia, which is not easy in practice to perform osteotomies without detaching the flap from the rest of the leg.

In our study, we have proposed to use bone surface marking as a registration method, with an accuracy < 1 mm. As we fixed a tracked marker on the fibula, the fibula could be detached from the tibia and the osteotomies performed once the fibula is released from its attachments on the leg.

Some details of this fibular registration method will have to be further studied before its use in clinical practice. First, a learning curve is essential for bone surfacing to be precise enough. Here, for it to be feasible, the bone must be exposed, i.e. cleared of all muscle attachments to be able to digitalize its surface. The surgeon will then be able to conscientiously carry out the surfacing on the bare bone, in order to get a point cloud that reproduces correctly the bone surface. The duration of the procedure also has to be taken into account. As for many navigation methods, this bone surfacing procedure is quite time-consuming despite the fact that navigation is meant to help the surgeon in his/her task and thus ultimately to gain time. This point will have to be evaluated in a clinical study to determine the amount of time required for implementing a fibula flap design with navigation (including both the bone exposure and navigation time, minus the gain of time due to the navigation assistance) compared to that without navigation. Finally, the ideal positioning of the tracked marker on the fibula will have to be studied so as not to interfere either with osteotomies or with the surface digitization. The marker will obviously have to be located in the SEA, on one of its extremities. We will study in the ongoing work the practical and ergonomic aspect of its rather proximal or distal positioning on the SEA.

Concerning the initialization phase, our RIP method is based on measurements between the malleolus extremity and the fibula borders. It has been shown to be precise enough for registration but this will have to be assessed on human fibulas. The RIPs will thus have to be digitized before detachment of the fibula from its malleolus but following surgical exposure of the lateral part of the fibula. The distal extremity of the fibula will have to be located by manual palpation through the skin, which would not be problematic in most patients but could be in overweight patients or others with edema of the lower limbs [31,32]. In such cases, intraoperative ultrasound location of the fibula distal extremity could then be easily used. We choose to not use the distal extremity of the fibula directly as an initialization point because the accuracy of its localization would be dependent of the patients' characteristics. Indeed, the skin interface between the malleolus and the tracked tool tip would in some patients be relatively large (from a few millimeters to several centimeters because of lymphoedema or obesity for example [31,32]). On a 3D printed model the skin interface issue would not have been a problem, but it would be one on a patient. Using points remoted from this distal extremity but placed on the fibula bone makes it possible at least to limit the transverse and sagittal errors since the tracked tool tip is in direct contact with the bone. For these reasons, we have preferred this RIPs approach.

Finally, the cost of this registration method will now have to be evaluated. A medico-economic study should be carried out to evaluate the cost of this navigation method. This cost should then be compared to the ones of a fibula flap (i) without guidance and (ii) with manufactured cutting guides.

Conclusion

This study highlighted the relevance of the concept of bone surface matching on a fibula using an ICP-based registration method, despite the absence of anatomical landmarks on the fibula. We have proposed a registration initialization method based on initialization points located on the fibula diaphysis and remote from the distal extremity of its malleolus. The registration was successfully achieved with a mean accuracy of 0.759 ± 0.302 mm. These findings indicate that navigation and computer-assisted surgery tools could be used for shaping of the fibula flap for mandibular reconstruction using a noninvasive and accurate registration method. Ongoing studies are under way to evaluate this bone surface-matching registration method on cadavers and then to develop and evaluate navigation-guided fibular osteotomies on cadavers and in clinical practice.

Compliance with ethical standards

Conflict of interest The authors declare that they have no conflict of interest.

Ethical approval For this type of study formal consent is not required.

References

1. Hidalgo DA. Fibula free flap: a new method of mandible reconstruction (1989) *Plast Reconstr Surg* 84(1):71–9.
2. Moro A, Cannas R, Boniello R, Gasparini G, Pelo S (2009) Techniques on modeling the vascularized free fibula flap in mandibular reconstruction. *J Craniofac Surg* 20(5):1571–3. <https://doi.org/10.1097/SCS.0b013e3181b0db5c>

3. Thankappan K, Trivedi NP, Subash P, Pullara SK, Peter S, Kuriakose MA, Subramania I (2008) Three-dimensional computed tomography-based contouring of a free fibula bone graft for mandibular reconstruction. *J Oral Maxillofac Surg* 66(10):2185–92. <https://doi.org/10.1016/j.joms.2008.01.035>
4. Blackwell KE, Brown MT, Gonzalez D (1997) Overcoming the learning curve in microvascular head and neck reconstruction. *Arch Otolaryngol Head Neck Surg* 123(12):1332–5. <https://doi.org/10.1001/archotol.1997.01900120082013>
5. Zhang L, Liu Z, Li B, Yu H, Shen SG, Wang X (2016) Evaluation of computer-assisted mandibular reconstruction with vascularized fibular flap compared to conventional surgery. *Oral Surg Oral Med Oral Pathol Oral Radiol* 121(2):139–48. <https://doi.org/10.1016/j.oooo.2015.10.005>
6. Bosc R, Hersant B, Carloni R, Niddam J, Bouhassira J, De Kermadec H, Bequignon E, Wojcik T, Julieron M, Meningaud J-P (2017) Mandibular reconstruction after cancer: an in-house approach to manufacturing cutting guides. *Int J Oral Maxillofac Surg* 46(1):24–31. <https://doi.org/10.1016/j.ijom.2016.10.004>
7. Bao T, He J, Yu C, Zhao W, Lin Y, Wang H, Liu J, Zhu H (2017) Utilization of a pre-bent plate-positioning surgical guide system in precise mandibular reconstruction with a free fibula flap. *Oral Oncol* 75:133–9. <https://doi.org/10.1016/j.oraloncology.2017.11.011>
8. Li P, Xuan M, Liao C, Tang W, Wang X-Y, Tian W, Long J (2016) Application of intraoperative navigation for the reconstruction of mandibular defects with microvascular fibular flaps-preliminary clinical experiences. *J Craniofac Surg* 27(3):751–5. <https://doi.org/10.1097/SCS.0000000000002430>
9. Zhou C, Anschuetz L, Weder S, Xie L, Caversaccio M, Weber S, Williamson T (2016) Surface matching for high-accuracy registration of the lateral skull base. *Int J Comput Assist Radiol Surg* 11(11):2097–103. <https://doi.org/10.1007/s11548-016-1394-3>
10. Shan X-F, Chen H-M, Liang J, Huang J-W, Zhang L, Cai Z-G, Guo C (2016) Surgical navigation-assisted mandibular reconstruction with fibula flaps. *Int J Oral Maxillofac Surg* 45(4):448–53. <https://doi.org/10.1016/j.ijom.2015.08.1006>
11. Yu Y, Zhang W-B, Liu X-J, Guo C-B, Yu G-Y, Peng X (2016) A new procedure assisted by digital techniques for secondary mandibular reconstruction with free fibula flap. *J Craniofac Surg* 27(8):2009–14. <https://doi.org/10.1097/SCS.0000000000003096>
12. Shen S-Y, Yu Y, Zhang W-B, Liu X-J, Peng X (2017) Angle-to-angle mandibular defect reconstruction with fibula flap by using a mandibular fixation device and surgical navigation. *J Craniofac Surg* 28(6):1486–91. <https://doi.org/10.1097/SCS.0000000000003891>
13. Pietruski P, Majak M, Świątek-Najwer E, Żuk M, Popek M, Mazurek M, Świecka M, Jaworowski J (2019) Navigation-guided fibula free flap for mandibular reconstruction: A proof of concept study. *J Plast Reconstr Aesthet Surg*. 72(4):572-580 <https://doi.org/10.1016/j.bjps.2019.01.026>
14. Luebbbers H-T, Messmer P, Obwegeser JA, Zwahlen RA, Kikinis R, Graetz KW, Matthews F (2008) Comparison of different registration methods for surgical navigation in cranio-maxillofacial surgery. *J Craniomaxfac Surg* 36(2):109–16. <https://doi.org/10.1016/j.jcms.2007.09.002>
15. Strong EB, Tollefson TT (2013) Intraoperative use of CT imaging. *Otolaryngol Clin North Am* 46(5):719–32. <https://doi.org/10.1016/j.otc.2013.07.003>
16. 3D Slicer (2021) 3D Slicer image computing platform. Available from: <https://www.slicer.org/>
17. Yaniv Z (2015) Which pivot calibration? *Medical Imaging: Image-Guided Procedures, Robotic Interventions, and Modeling* p. 941527. <https://doi.org/10.1117/12.2081348>
18. CloudCompare (2022) Open Source project [Internet]. <http://www.cloudcompare.org/>. Accessed 9 March 2022
19. Jones MW, Baerentzen JA, Sramek M (2006) 3D distance fields: a survey of techniques and applications. *IEEE Trans Vis Comput Graphics* 12(4):581-599. <https://doi.org/10.1109/TVCG.2006.56>.
20. Besl PJ, McKay ND (1992) A method for registration of 3-D shapes. *IEEE Trans Pattern Anal Mach Intell* 14(2):239-256. <https://doi.org/10.1109/34.121791>
21. Cignoni P, Rocchini C, Scopigno R (1998) Metro: measuring error on simplified surfaces *Comput Graphics Forum* 17(2):167–74. <https://doi.org/10.1111/1467-8659.00236>
22. Girardeau-Montaut D (2006) Détection de changement sur des données géométriques tridimensionnelles *Dissertation, Paris, ENST*. <https://www.theses.fr/2006ENST0005>.
23. Distances Computation (2021) CloudCompareWiki [Internet] Available from: http://www.cloudcompare.org/doc/wiki/index.php?title=Distances_Computation. Accessed 9 March 2022

24. Kamio T, Hayashi K, Onda T, Takaki T, Shibahara T, Yakushiji T, Shibui T, Kato H (2018) Utilizing a low-cost desktop 3D printer to develop a 'one-stop 3D printing lab' for oral and maxillofacial surgery and dentistry fields. *3D Print Med* 4(1):6. <https://doi.org/10.1186/s41205-018-0028-5>
25. Damecourt A, Nieto N, Galmiche S, Garrel R, de Boutray M (2020) In-house 3D treatment planning for mandibular reconstruction by free fibula flap in cancer: Our technique. *Eur Ann Otorhinolaryngol Head Neck Dis* 137(6):501–5. <https://doi.org/10.1016/j.anorl.2020.02.002>
26. Yuan X, Xuan M, Tian W, Long J (2016) Application of digital surgical guides in mandibular resection and reconstruction with fibula flaps. *Int J Oral Maxillofac Surg* 45(11):1406–9. <https://doi.org/10.1016/j.ijom.2016.06.022>
27. Rommel N, Kesting MR, Rohleder NH, Bauer FMJ, Wolff K-D, Weitz J (2017) Mandible reconstruction with free fibula flaps: Outcome of a cost-effective individual planning concept compared with virtual surgical planning. *J Craniomaxillofac Surg*. 45(8):1246–50. <https://doi.org/10.1016/j.jcms.2017.04.010>
28. Widmann G, Stoffner R, Bale R (2009) Errors and error management in image-guided craniomaxillofacial surgery. *Oral Surg Oral Med Oral Pathol Oral Radiol Endod* 107(5):701–15. <https://doi.org/10.1016/j.tripleo.2009.02.011>
29. Lefèvre E, Farlay D, Bala Y, Subtil F, Wolfram U, Rizzo S, Baron C, Zysset P, Pithioux M, Follet H (2019) Compositional and mechanical properties of growing cortical bone tissue: a study of the human fibula. *Sci Rep* 9:17629 <https://doi.org/10.1038/s41598-019-54016-1>
30. Fusion track 500 (2021) Actrasys measurement products [Internet]. Available from: <https://www.actrasys-measurement.com/products/fusiontrack-500>. Accessed 9 March 2022
31. Evans NS, Ratchford EV (2016) The swollen leg. *Vasc Med*. 21(6):562–4. <https://doi.org/10.1177/1358863X16672576>
32. Perrin M, Guex JJ (2000) Edema and leg volume: methods of assessment. *Angiology*. 51(1):9–12. <https://doi.org/10.1177/000331970005100103>